Optics Communications 283 (2010) 2301–2307

Contents lists available at ScienceDirect

Optics Communications

journal homepage: www.elsevier.com/locate/optcom

Low noise spinning wheel technique for THz material parameter extraction

Jegathisvaran Balakrishnan [a,*], Bernd M. Fischer [a,b], Derek Abbott [a]

[a] Centre for Biomedical Engineering and School of Electrical & Electronic Engineering, The University of Adelaide, Adelaide, SA 5005, Australia
[b] Division IV, ERG, French-German Research Institute of Saint Louis (ISL), BP 70034, 68301 Saint Louis Cedex, France

ARTICLE INFO

Article history:
Received 17 November 2009
Received in revised form 4 January 2010
Accepted 19 January 2010

Keywords:
T-rays
Terahertz
Double-modulated THz-DTDS
Differential time-domain spectroscopy

ABSTRACT

Double-modulated terahertz differential time-domain spectroscopy (double-modulated THz-DTDS), is a technique that is based on dithering the sample under test. In this paper, we report a measurement technique based on mounting the sample on a spinning wheel, in order to overcome fundamental limitations imposed by linear dithering. We demonstrate a proof-of-principle showing that noise decreases as a function of the spinning wheel modulation frequency. This technique does not suffer the mechanical noise limitation of traditional linear dithering and thus opens up future scope for further noise reduction via hardware advances in the modulation frequency of the wheel. The spinning wheel technique enables a rapid succession of measurements between the reference and sample signals with a single mechanical delay scan. As a result, an improvement in measurement time by at least a factor of two, as compared to the conventional THz-TDS measurement technique is observed. The spinning wheel technique is experimentally verified by measuring the dielectric properties of a thick polymer material.

1. Introduction

The rapidly evolving area of terahertz (T-ray) technology has drawn considerable attention for a variety of applications. Terahertz is currently of great interest in applications such as medical diagnostics [1,2], chemical and biological identification [3,4], and quality control [5]. Due to the advent of THz technology, the measurement techniques used in conventional THz-TDS are still far less developed as compared to other well-developed electromagnetic technologies such as MRI and X-rays. In a typical conventional THz-TDS setup, a complete scan consists of a reference (air) scan and a sample (material) scan. In order to obtain a high SNR, each scan requires a separate delay stage scan with a measurement time of several minutes depending on the time constant set by the lock-in amplifier. A number of significant studies have motivated the need for a fast and reliable THz measurement technique, including: fast scanning of terahertz signal using oscillating and rotary optical delay lines [6,7], real-time terahertz scanner for moving objects, rapid-phase modulation for high speed terahertz imaging and spectroscopy [8], and simultaneous reference and differential waveform acquisition [9].

In this paper, we demonstrate simulation and experimental results of a spinning wheel technique implemented using a double-modulated terahertz differential time-domain spectroscopy (double-modulated THz-DTDS) experimental setup [10]. The spinning wheel technique enables a rapid succession of measurements between the reference and sample signals with a single delay stage scan. This technique allows an improvement in the reference and sample measurement times by at least a factor of two as compared to the conventional THz-TDS measurement technique. The spinning wheel technique is experimentally verified using a polyvinyl chloride (PVC) polymer sample under test. A standardized sample thickness of 3 mm is used herein and this is a trade-off between maximising bandwidth and maximising THz interaction depth in the samples.

2. THz-DTDS and double-modulated THz-DTDS

THz-DTDS is an experimental setup [11] based on a differential signal measurement. The THz-DTDS setup was first used to measure the dielectric and optical properties of nanometer scaled dielectric films in the THz frequency band. The dielectric film is mounted on a hammer-like sample holder that is designed to be half coated and half uncoated with a thin sample film on a substrate (Fig. 1). The sample holder is mounted on a galvanometer operating at f_{shaker} set at 16 Hz. Therefore, as the THz (T-ray) beam transmits through the dithered sample, a differential signal can be generated. Dithering the sample holder by covering the half coated thin film by a metal plate generates a differential reference signal. Thus, by taking the ratio of the differential signal over the differential reference signal, dielectric and optical properties of the sample film can be determined. Recently, Mickan et al. [12] and Kwang et al. [13], investigated a double-modulated THz-DTDS technique whereby a double modulation scheme is used to extract the

* Corresponding author.
E-mail address: jega@eleceng.adelaide.edu.au (J. Balakrishnan).

0030-4018/$ - see front matter Crown Copyright © 2010 Published by Elsevier B.V. All rights reserved.
doi:10.1016/j.optcom.2010.01.042

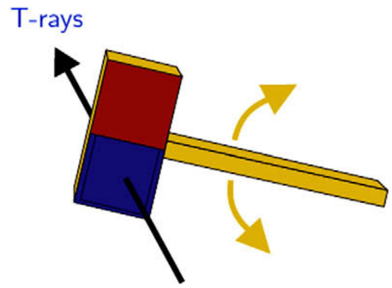

Fig. 1. The hammer-like sample holder for a differential measurement technique. The sample holder is half coated and half uncoated with a thin film on a substrate, serving as sample and reference [11-14].

differential signal and the differential reference signal of a thin film. According to Mickan et al. [12], the double modulation technique is analogous to encoding information on a carrier wave in a radio system. Here, the modulated THz signal at lower frequency, f_{shaker}, is further modulated at a higher frequency, $f_{chopper}$. The double-modulated THz signal is then demodulated using two separate lock-in amplifiers. The first lock-in amplifier is demodulated at $f_{chopper}$ to remove the carrier frequency component. Here, the lock-in amplifier is set to a low time constant to minimise the filtering effect. The output of the lock-in amplifier is then fed into the second lock-in amplifier. The second lock-in amplifier demodulates at f_{shaker} to produce the differential signal. The process is repeated for a differential reference measurement with the sample thin film covered by a metal plate thereby blocking the THz beam. In this case, an improvement in the shaking frequency of up to 66 Hz is achieved. In 2002, Mickan et al. [14] reported the use of double-modulated DTDS for bioaffinity sensing. In this work, a surface recognition process of a highly specific label-free biotin-avidin complex was investigated. Furthermore, double-modulated THz-DTDS can be used for measuring thin liquid layers [10]. In that work, simultaneous dual-waveform acquisition, resulting in mean and amplitude signals, are introduced for the first time. The dual-waveform acquisition is implemented using an audio speaker to dither the sample.

Although working measurement techniques implemented with THz-DTDS or double-modulated THz-DTDS have been demonstrated, the limitation caused by the mechanical instability of the dithering mechanism introduces noise into the system. Furthermore, prior measurement techniques [10–14] can be time consuming especially in terms of sample preparation and measurement scan time—laser drift can be an issue, especially during the sample preparation period, since two separate scans are required to determine the dielectric properties of a material. Recently, several preliminary studies have been conducted by Balakrishnan et al. [15–18] on double-modulated THz-DTDS using a spinning wheel technique with simultaneous dual-waveform acquisition for measuring the dielectric properties of a material, however no detailed studies have been described so far.

Thus, in this paper, we describe a detailed study of a spinning wheel technique with simultaneous dual-waveform acquisition for potentially improving the noise performance. Both simulation and experimental results of the spinning wheel technique are presented.

3. Spinning wheel

The spinning wheel (Fig. 2) is a mechanism we now introduce to address the mechanical instability in the prior linear dithering technique. The spinning wheel is designed to measure the reference and sample signals in quick succession with a single mechanical delay scan. The spinning wheel consists of five main parts: sample holder, sample material, photointerrupter and interrupter disc, rpm to Hz converter circuit and brushless DC motor set which consists of pulley, timing belt, high speed three-phase DC motor, and speed controller. The sample holder is built using a robust stainless steel wheel supported by low friction ball bearings. The wheel is driven by a high speed brushless DC motor with a built-in governor mode. The governor mode is enabled to allow the motor to operate at a fixed speed. A custom-built pulley, a timing belt and a speed controller are attached to the motor. The sample is designed with half reference (air) and half sample (polymer) as shown in Fig. 3. This design allows a rapid succession of measurements between reference and sample as the wheel spins. A photointerrupter electronic circuit and a photointerrupter disc, which are used to convert the wheel's spinning speed (rpm) into

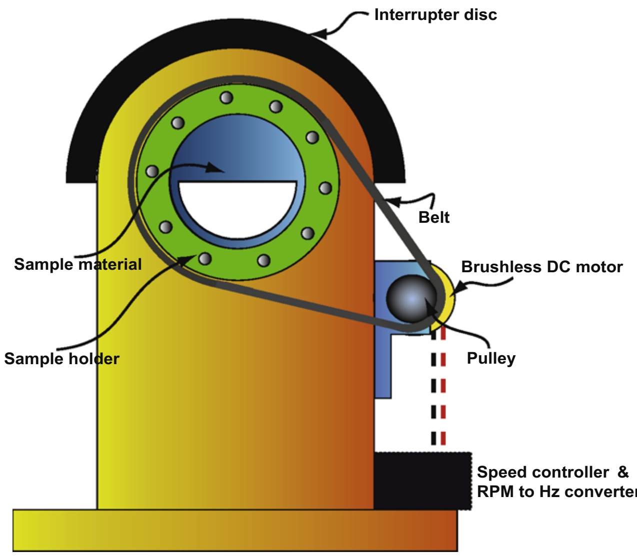

Fig. 2. Spinning wheel for double-modulated THz-DTDS polymer measurements. The spinning wheel is located in the focal plane with a frequency setting of upto 310 Hz. As THz transmits through the rotating sample, a rapid succesion of measurements can be achieved.

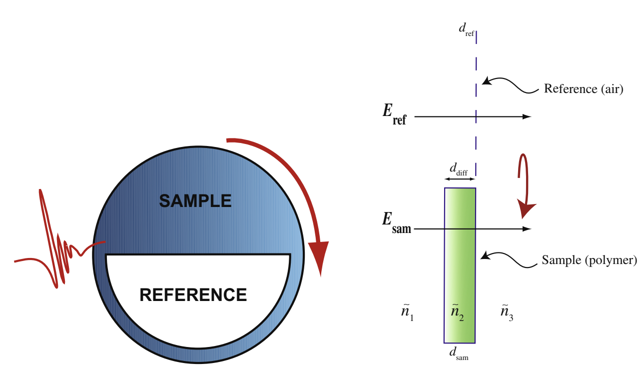

(a) Front view of sample material

(b) Cross-section of sample material

Fig. 3. Polymer sample design for a double-modulated THz-DTDS measurement. This figure depicts the sample under test in the double-modulated DTDS measurement. In (a), the test sample is designed to be half reference (air) and half sample (polymer) and it is mounted onto the spinning wheel as shown in and half sample (polymer) and it is mounted onto the spinning wheel as shown in $\tilde{\eta}_1$ and $\tilde{\eta}_2$ are the refractive index of air, and $\tilde{\eta}_2$ is the refractive index of the sample material. Here, $d_{diff} = d_{sam} - d_{ref}$ is the thickness of the sample material. The electric field components for reference and sample signals are denoted as E_{ref} and E_{sam} respectively.

frequency (Hz) are attached to the spinning wheel. Hence, the wheel is placed in the double-modulated THz-DTDS experimental setup described in Fig. 7 for a measurement. Transmitting THz beam through the rapidly rotated sample produces a rapid succession of measurements. The time between measuring the reference and sample is thereby dramatically reduced and is determined by the speed of the wheel.

4. Simulation

The rapid succession measurement using the spinning wheel technique is simulated using Matlab based on the flow chart presented in Fig. 4. The detected double-modulated THz signal at nth step is denoted as $E_{\mathrm{dm}}(\tau_{\mathrm{n}})$,

$$E_{\mathrm{dm}}(\tau_{\mathrm{n}}) = A_{\tau_{\mathrm{n}}}\left(\left(1+\frac{4}{\pi}\sum_{k=1}^{\infty}\frac{\sin(2k-1)\omega_{\mathrm{chopper}}t+\phi_{\mathrm{chopper}}}{(2k-1)}\right)\times\left(\frac{x-d}{x}\left(1+\frac{4}{\pi}\sum_{k=1}^{\infty}\frac{\sin(2k-1)\omega_{\mathrm{wheel}}t+\phi_{\mathrm{wheel}}}{(2k-1)}\right)+d\right)\right), \tag{1}$$

where $A_{\tau_{\mathrm{n}}}$ is the averaged amplitude with varying time delay, τ_{n} and n is the step number determined by the delay stage. Here, x is the thickness of the reference signal. The sample material thickness is defined as d. Here, the $\omega_{\mathrm{chopper}} = \frac{1}{4}2\pi f_{\mathrm{chopper}}$ and $\omega_{\mathrm{wheel}} = \frac{1}{4}2\pi f_{\mathrm{wheel}}$ represent the chopper frequency and the spinning wheel frequency respectively. Also, ϕ_{chopper} refers to the chopper phase and ϕ_{wheel} refers to wheel phase. The detected double-modulated signal is further amplified using a low-noise pre-amplifier before entering the 2-way power splitter. The time delay dependant amplified signal, $E_{\mathrm{p}}(\tau_{\mathrm{n}})$ can be written as follows:

$$E_{\mathrm{p}}(\tau_{\mathrm{n}}) = A_g E_{\mathrm{dm}}(\tau_{\mathrm{n}}), \tag{2}$$

where A_g denotes the gain applied to the detected signal. The amplified signal is then split using a 2-way power splitter to produce the split signals, $E_{\mathrm{s_1}}(\tau_{\mathrm{n}})$ and $E_{\mathrm{s_2}}(\tau_{\mathrm{n}})$. These signals enter the input channel of the lock-in amplifier one (LIA1) and the $X_{\mathrm{modulator}}$ input channel of the mixer respectively. The $E_{\mathrm{s_1}}(\tau_{\mathrm{n}})$ and $E_{\mathrm{s_2}}(\tau_{\mathrm{n}})$ are described as follows:

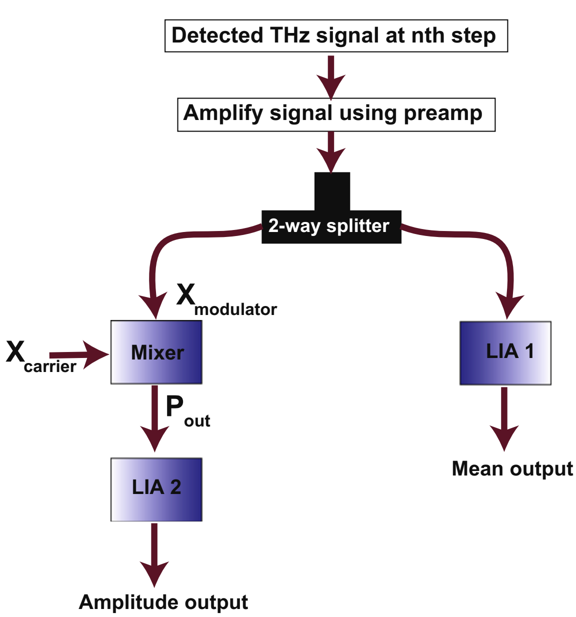

Fig. 4. Flowchart of the simulation process for mean and amplitude signal extraction. The detailed explanation of the flowchart is given in the text.

$$E_{\mathrm{s_1}}(\tau_{\mathrm{n}}) = E_{\mathrm{s_2}}(\tau_{\mathrm{n}}) = \frac{1}{2}E_{\mathrm{p}}(\tau_{\mathrm{n}}). \tag{3}$$

As the input channel of LIA1 receives the $E_{\mathrm{s_1}}(\tau_{\mathrm{n}})$ from the splitter, the external chopper reference signal, $E_{\mathrm{c}}(t)$ with phase ϕ_c is fed into the reference input channel of LIA1 simultaneously for signal demodulation. The external chopper signal, $E_{\mathrm{c}}(t)$ is given by,

$$E_{\mathrm{c}}(t) = 1+\left(\sum\nolimits_{k=1}^{\infty}\frac{\sin((2k-1)\omega_{\mathrm{c}}t+\phi_{\mathrm{c}})}{(2k-1)}\right), \tag{4}$$

where $\omega_c = 2\pi f_c$ is the reference frequency with phase, ϕ_c. Assuming that the chopper phase, ϕ_{chopper}, is synchronised to ϕ_c and the chopper frequency, $\omega_{\mathrm{chopper}}$ is synchronised to ω_c, the double-modulated signal is frequency shifted after the demodulation stage. The demodulated output is then low-pass filtered to remove the unwanted frequency components. Thus, the output signal detected at LIA1 is denoted as the time delay dependant mean signal, $E_{\mathrm{mean}}(\tau_{\mathrm{n}})$. The mixer illustrated in Fig. 4 is used as a multiplier. It consists of two input channels, $X_{\mathrm{modulator}}$ and X_{carrier}, and an output channel P_{out}. Here, P_{out} is the product of $X_{\mathrm{modulator}}$ and X_{carrier} input channels. Therefore, as the double-modulated signal from the splitter, $E_{\mathrm{s_2}}(\tau_{\mathrm{n}})$ enters $X_{\mathrm{modulator}}$ and the external chopper reference signal, $E_{\mathrm{c}}(t)$ fed into X_{carrier} input channel simultaneously, a frequency shifting effect can be observed at the output channel of the mixer. Fig. 5 shows the simulation-based frequency shifting effect at the mixer output channel.

Here, the mixer is designed without any filters. Therefore, the output of the mixer consists of frequency shifted components and noise. The mixer output, $P_{\mathrm{out}}(\tau_{\mathrm{n}})$ is then fed into the second lock-in amplifier (LIA2). Here, LIA2 further demodulates the output signal from the mixer with wheel reference signal, $E_{\mathrm{w}}(t)$. The $E_{\mathrm{w}}(t)$ can be deduced as follows:

$$E_{\mathrm{w}}(t) = 1+\left(\sum\nolimits_{k=1}^{\infty}\frac{\sin((2k-1)\omega_{\mathrm{w}}t+\phi_{\mathrm{w}})}{(2k-1)}\right), \tag{5}$$

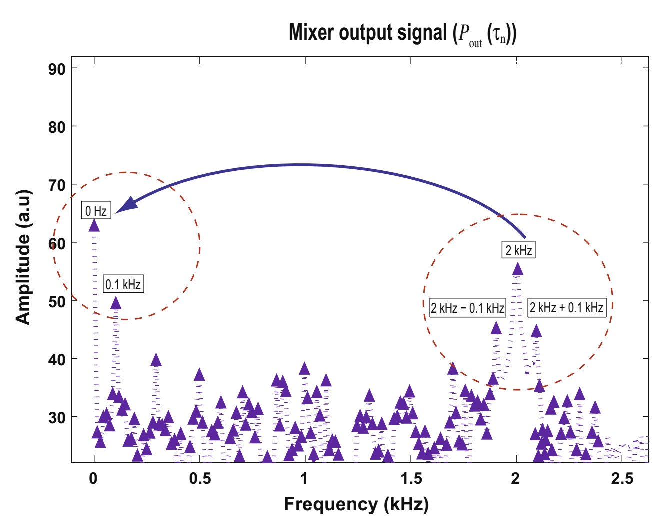

Fig. 5. Simulated mixer output at nth step of the delay stage in frequency domain. This figure illustrates the product of $X_{\mathrm{modulator}}$ and X_{carrier} channels of the mixer at the nth step of the delay stage in frequency domain. The $X_{\mathrm{modulator}}$ input channel is fed with the simulated double-modulated signal, $E_{s2}(\tau_n)$ with f_{chopper} of 2 kHz and f_{wheel} of 0.1 kHz and the X_{carrier} input channel is fed with the simulated chopper reference signal $E_c(t)$ with f_c of 2 kHz. Thus, the simulated $E_{s2}(\tau_n)$ consists of a sum component (2 + 0.1 kHz) and a difference component (2 – 0.1 kHz) is frequency shifted as illustrated in the figure above. With the assumption that the phase and frequency components of $E_{s2}(\tau_n)$ synchronises to the phase and frequency components of $E_c(t)$, one can deduce the output of the mixer, $P_{\mathrm{out}}(\tau_n)$ as shown in the figure. Therefore, the simulated double-modulated signal will be shifted towards the DC at the output of the mixer. The shifted components will then enter the input channel of LIA2 for further demodulation process to produce the amplitude signal.

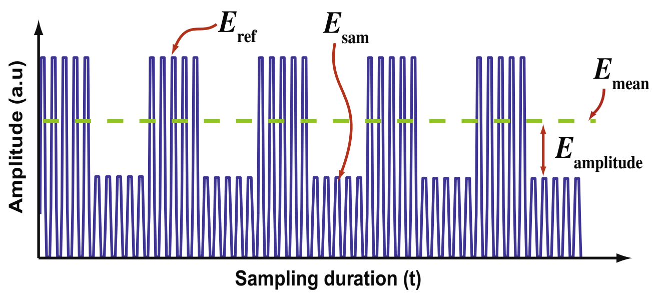

Fig. 6. Time-domain simulated output signal of a mixer at *n*th step of the delay stage. This figure depicts a simulated output of the mixer at nth step of the delay stage. A rapid succesion of measurements produce a square wave pattern at the output of the mixer. This square wave consists of reference signal, $E_{ref}(\tau_n)$, sample signal, $E_{sam}(\tau_n)$, mean signal, $E_{mean}(\tau_n)$, and amplitude signal, $E_{amplitude}(\tau_n)$.

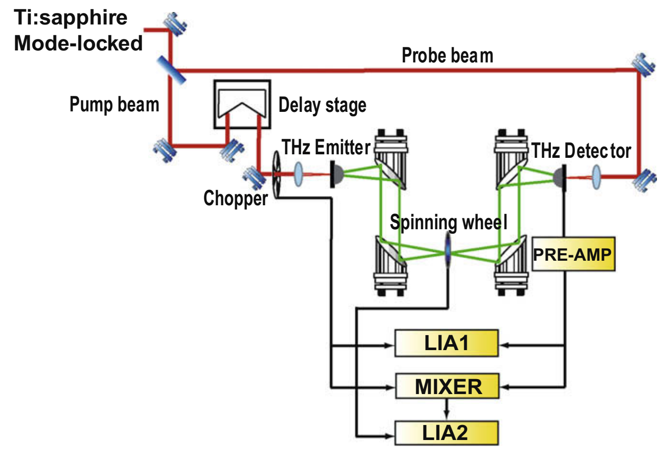

Fig. 7. Double-modulated THz-DTDS spectrometer schematic for polymer materials measurement. This schematic diagram illustrates a double-modulated DTDS spectrometer configured for characterizing dielectric properties of polymer materials. The sample material placed at the focal plane is modulated at f_{wheel} of 66–310 Hz. A Ti-sapphire femtosecond laser is split into pump beam and probe beam. The pump beam is modulated at 2.2 kHz using a mechanical chopper and focused on an emitting photoconductive antenna to generate THz pulse. The THz pulse is collimated and focused onto the rotating sample. The transmitted THz pulse is recollimated and focused onto the photoconductive detector antenna. The probe beam gates the incoming THz pulse at the detector. The detected THz pulse is pre-amplified and fed into lock-in amplifiers and mixer for mean and amplitude signals extraction.

where $\omega_w = 2\pi f_w$ is the reference frequency with phase, ϕ_w. With an assumption that the phase, ϕ_{wheel} is synchronised to the phase of the wheel reference signal, ϕ_w and the wheel frequency, ω_{wheel} is synchronised to ω_w, the demodulated mixer output is further frequency shifted after the demodulation process. Thus, the demodulated signal is low-pass filtered to produce the time delay dependant amplitude signal, $E_{amplitude}(\tau_n)$ at the output of LIA2. Therefore, with the extracted mean and amplitude signals, the reference and sample signals can be obtained. Further explanation of the reference signal and sample signal extraction is described in the analysis section. Fig. 6 shows the simulated time-domain output signal of the mixer at *n*th step of the delay stage. In this figure, the relationships between the mean, amplitude, reference, and sample signals are depicted.

5. Experimental method

The double-modulated DTDS setup for a polymer material measurement is shown in Fig. 7. A Mira-SEED Ti-sapphire femtosecond mode-locked laser is used as a source of optical pulses. It is pumped by Verdi V6 laser with a wavelength of 532 nm. The femtosecond laser produces an output pulse duration of 20 fs at a repetition rate of 76 MHz. This laser has an output power of 1 W with a centered wavelength at 800 nm. The laser is split into a pump beam and a probe beam using a beamsplitter. The pump beam is modulated by an optical chopper at a frequency of 2.2 kHz. The modulated beam is then focused on an emitting photoconductive antenna using a plano-convex optical lens. The emitting antenna is biased at 90 Vdc using a standard low current power supply. The modulated beam is incident on the emitter for generating the THz pulse. The THz pulse is collimated and focused onto the rotating polymer material using the first pair of off-axis parabolic mirrors. Here, the spinning wheel speed is set to a frequency range of 66 Hz to 310 Hz. The THz pulse transmits through the rotating sample and is recollimated and focused onto the photoconductive detector antenna using the second pair of off-axis parabolic mirrors. The probe beam gates the transmitted THz pulse by focusing the laser beam onto the photoconductive antenna at the detector. Two SR830 lock-in amplifiers, a low-noise SR560 pre-amplifier and a custom-built electronic mixer based on an MC1495P multiplier chip are used for signal extraction in this setup. The details of the signal extraction are given in the following section.

5.1. Lock-in amplifier configuration

The lock-in amplifier configuration for mean and amplitude signal extraction is shown in Fig. 8. First, the detected double-modulated THz signal is fed into the pre-amplifier for signal amplification. The amplified signal is then fed into a low-noise 2-way power splitter. Thus, one end of the splitter output is connected to the input channel of the first lock-in amplifier (LIA1) and the other end of splitter output is fed into the $X_{modulator}$ input channel of the mixer. Here, the LIA1 input signal is demodulated using the external chopper reference signal. Autophasing the LIA1 input signal to the external chopper reference signal synchronizes the phase of the input signal to the phase of the external chopper reference signal. Thus, synchronised signals are low-pass filtered to produce a mean signal, $E_{mean}(\tau_n)$ at the output channel of LIA1. The MC1495P mixer input signal is demodulated with the external chopper reference signal, however, no filtering is applied to the output signal of the mixer. As a result, the output of the mixer consists of frequency shifted components and noise as described in Fig. 5. The mixer has the facility for applying this scaling factor via an external variable resistor. The scaled output of the mixer is fed into the input channel of LIA2. The input signal is then demodulated using the external wheel reference signal. Autophas-

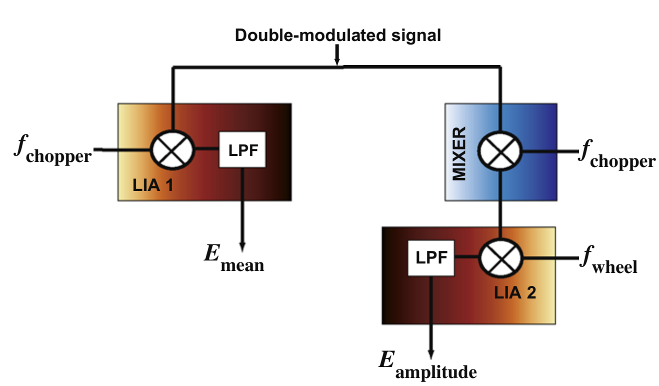

Fig. 8. Lock-in amplifier configuration for mean and amplitude signals extraction. This figure shows a simulataneous dual-waveform acquisition (mean and amplitude) using two lock-in amplifiers and a mixer. The detailed explanation of the lock-in amplifier configuration is given in the text.

ing the input signal to the wheel reference signal, synchronizes the phase of the wheel reference signal with the input signal. The synchronised signals are then low-pass filtered to produce an amplitude signal, $E_{\text{amplitude}}(\tau_n)$ at the output channel of LIA2. Therefore, with the extracted mean and amplitude information, the reference and sample signals can be calculated according to Eqs. (6) and (7).

6. Analysis

Given that terahertz radiation is incident on the rotating sample, the mean and amplitude signals are then extracted according to the lock-in amplifier configuration described in Fig. 8. Therefore, based on the extracted mean and amplitude signals, the reference and sample signals can be calculated as follows [10]:

$$\widetilde{E}_{\text{ref}}(\omega) = \widetilde{E}_{\text{mean}}(\omega) + \widetilde{E}_{\text{amplitude}}(\omega), \tag{6}$$

$$\widetilde{E}_{\text{sam}}(\omega) = \widetilde{E}_{\text{mean}}(\omega) - \widetilde{E}_{\text{amplitude}}(\omega). \tag{7}$$

A spectral component of the reference and sample signals can be modelled based on the polymer material design presented in Fig. 3. Thus, the reference and sample signal can also be written as follows [19]:

$$\widetilde{E}_{\text{sam}}(\omega) = T_{12}(\omega) \cdot P_2(\omega, d_{\text{sam}}) \cdot T_{23}(\omega) \cdot A(\omega) \cdot \text{FP}(\omega), \tag{8}$$

$$\widetilde{E}_{\text{ref}}(\omega) = T_{13}(\omega) \cdot P_{\text{air}}(\omega, d_{\text{ref}}) \cdot A(\omega). \tag{9}$$

Hence, the complex transmission coefficient $T(\omega)$, is determined by taking the ratio of E_{sam} and E_{ref},

$$\widetilde{T}(\omega) = \frac{\widetilde{E}_{\text{sam}}(\omega)}{\widetilde{E}_{\text{ref}}(\omega)} = \rho e^{-j\phi}. \tag{10}$$

With the assumption that the complex refractive index of air, $\tilde{n}_1$ and $\tilde{n}_3 = 1$, the complex transmission coefficient can be simplified as follows:

$$\widetilde{T}(\omega) = \frac{4\tilde{n}_2(\omega)}{(1+\tilde{n}_2(\omega))^2} \exp\left(\frac{-i\,\omega\, d_{\text{diff}}}{c}(\tilde{n}_2(\omega) - 1)\right)\text{FP}(\omega), \tag{11}$$

where the frequency-dependant complex refractive index $\tilde{n}_2(\omega) = n_2(\omega) - j\kappa_2(\omega)$. Here, $n_2(\omega)$ and $\kappa_2(\omega)$ refer to the refractive index and extinction coefficient of the sample respectively. $d_{\text{diff}} = d_{\text{sam}} - d_{\text{ref}}$ where d_{sam} is the thickness of the sample material and d_{ref} is the thickness of the reference (Fig. 3b). The angular frequency is denoted as ω and the speed of light is denoted as c. The Fabry-Pérot reflection in the sample is labelled as $\text{FP}(\omega)$. According to Mickan et al. (2002) [12], the complex refractive index of a sample can be estimated by an iterative approximation or analytically. In our study, since the sample measured is sufficiently thick [20,21], the Fabry-Pérot reflections can be easily isolated. Thus, the analytic expression for n and κ can be made through approximation given in [22]. Here, we define the noise percentage, μ_x of the THz system as the standard deviation of the reference temporal electric field, ΔE_{ref} over the mean reference temporal electric field, E_{mref} [10,11]. The measurement is repeated five times for a noise percentage calculation. In this experiment, the lock-in amplifier time constant is set at 100 ms for both LIA1 and LIA2. The noise percentage, μ_x can be expressed as follows [10,11]:

$$\mu_x = \frac{\Delta E_{\text{ref}}}{E_{\text{mref}}} \times 100\%. \tag{12}$$

7. Results and discussion

As a proof-of-concept, the spinning wheel technique is experimentally verified using the following polymer material: polyvinyl chloride (PVC). The results obtained are compared with the results from a conventional THz-TDS measurement technique. From here on we have labelled the results obtained from the double-modulated spinning wheel as *double-modulated* and the results obtained from the conventional THz-TDS as *conventional*.

Polyvinyl chloride or in short PVC is a polar polymer that is optically opaque and its dielectric properties are well explored in terahertz range [20,23–25] as well as in the optical regime [26]. In this section, the dielectric properties of PVC in the terahertz band are measured using the double-modulated spinning wheel technique. The results obtained are then compared with the dielectric properties of PVC obtained from the conventional THz-TDS technique. These results agree well with the literature data [20,23,24]. At every nth step of the delay stage, reference and sample signals are measured in a rapid succession. This produces mean and amplitude waveforms simultaneously at the output channel of LIA1 and LIA2 (Fig. 9a).

Therefore, with the mean and amplitude signals, the reference and sample temporal electric field can be obtained by using the formulae given in Eqs. (6) and (7). In Fig. 9b, the double-modulated reference and sample waveforms are compared with the conventional reference and sample waveforms. A close match is observed between the double-modulated signals and the conventional signals. However, since the double-modulated and the conventional TDS measurements were not conducted simultaneously, a slight deviation is seen on the conventional TDS measurement. The deviation is mainly caused by the $1/f$ noise fluctuation originated from the mode-locked laser [27–29].

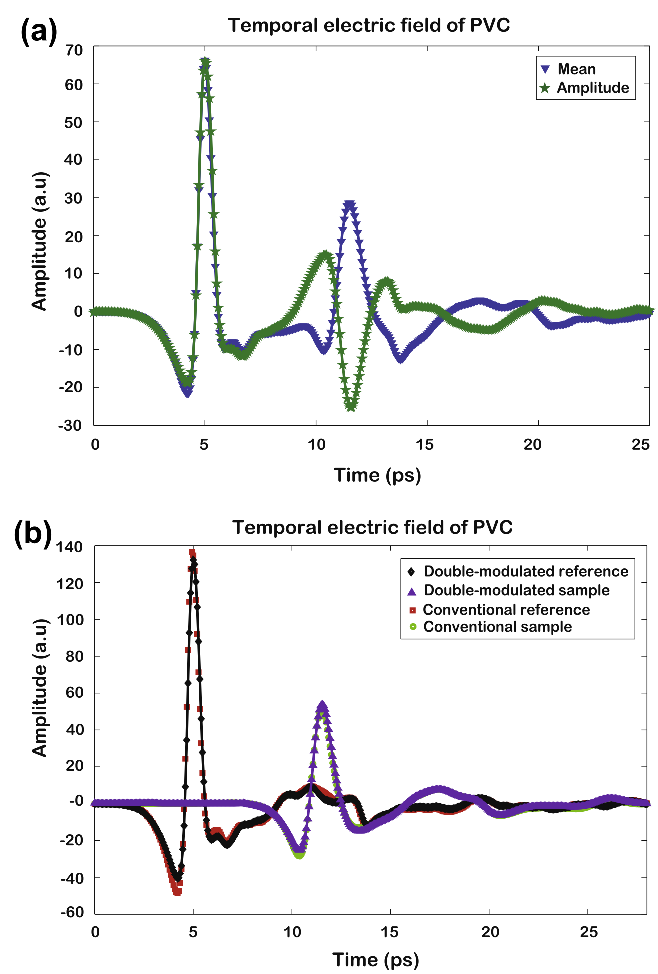

Fig. 9. Mean and amplitude waveforms of PVC. (a) The mean and amplitude waveforms of PVC obtained through the double-modulated DTDS technique and (b) The double-modulated and conventional reference and sample waveforms of PVC.

Fig. 10 compares the absorption coefficient, α, and refractive index, n, of PVC obtained through the double-modulated spinning wheel technique and conventional THz-TDS. In this measurement, the thickness of the sample under test is set at 3 mm to show proof-of- concept, however, measurement on a very thin sample can be carried out with an appropriate sample preparation technique.

In order to compare the noise performance of the double-modulated spinning wheel technique with conventional THz-TDS, five averages of reference scans are obtained and analysed according to the formula described in Eq. (12). Here, in order to calculate the noise percentage appropriately, we have only considered the fluctuations in the T-ray pulses, caused by the laser fluctuations. Thus, it is found that noise percentage, μ_x, of conventional THz-TDS is 1.84% as compared to 1.22% for the double-modulated spinning wheel technique. Here, the noise percentage of 1.22% is obtained when the spinning wheel is modulated at 310 Hz. Therefore, an improvement of 30% as compared to the conventional THz-TDS has been demonstrated. Thus, we confirm that the noise percentage present in the THz system can be reduced by using the spinning wheel technique. Fig. 11 shows the noise percentage of the THz system detected using the spinning technique as a function of modulation frequency. In this work, a preliminary result showing that the fluctuations in the T-ray pulses affected by the $1/f$ noise characteristic of the mode-locked laser can be improved by increasing the modulation frequency of the spinning wheel. Thus, the results presented in this work agree with the theoretical and experimental work presented in [10].

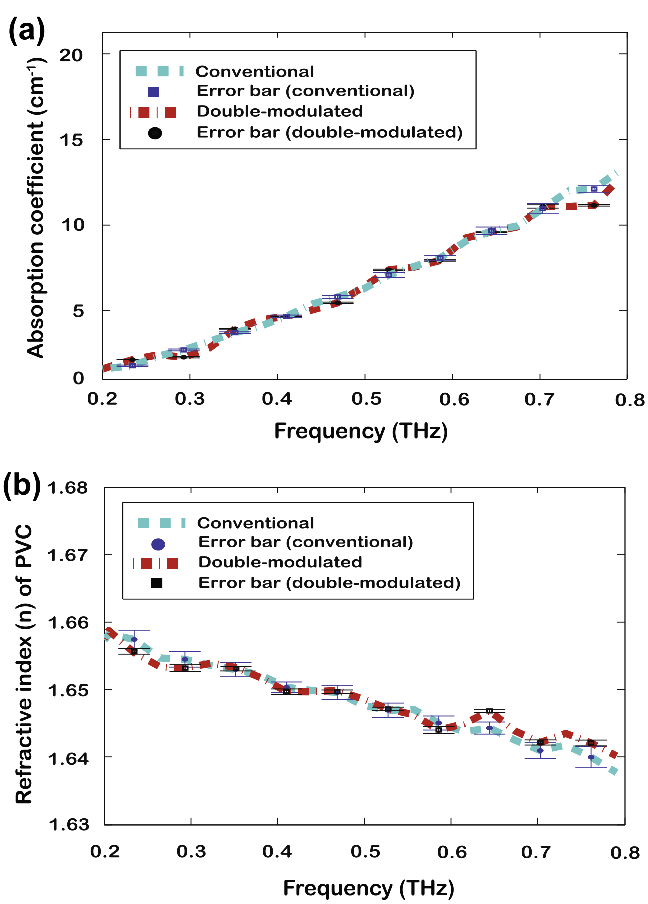

Fig. 10. Absorption coefficient and refractive index of PVC. This figure depicts the double-modulated and conventional absorption coefficient and refractive index of PVC, indicating a close match. The error bars indicate uncertainties in the conventional technique and double-modulated spinning wheel technique. According to the FFT of the temporal profile, it was observed that the linear region for the sample signal is limited to 0.8 THz and the signal is noisy thereafter.

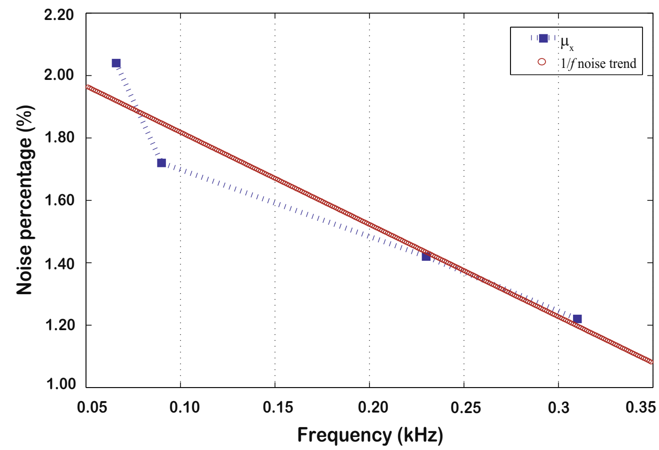

Fig. 11. Noise percentage, μ_x of the THz system detected using a spinning wheel technique as a function of modulation frequency. This figure illustrates that as the modulating frequency of the wheel increases, the noise present in the THz system reduces.

8. Conclusion

We develop a novel THz spinning wheel technique for material parameter measurement and demonstrate preliminary experimental results showing that the fluctuations in the T-ray pulses affected by the $1/f$ noise characteristic of the mode-locked laser can be improved by increasing the modulation frequency of the spinning wheel. This technique is successfully implemented using a double-modulated terahertz differential time-domain spectroscopy (double-modulated THz-DTDS) experimental setup. We demonstrate measurements in rapid succession, requiring one mechanical delay scan for the sample and reference signals. This results in a reduction in the measurement time of the reference and sample signals by at least a factor of two. We validate the technique using thick polymer test sample. A good agreement in the resulting dielectric parameters is produced when compared with the conventional THz-TDS technique. Thus, this demonstrates the accuracy of the double-modulated THz-DTDS spinning wheel technique. The noise level that is present in our double-modulated technique is lower than that in conventional TDS, especially as the modulating frequency of the wheel increases. An improvement of 30% as compared to the conventional THz-TDS has been demonstrated. The results herein represent proof-of-principle, and the noise level that is present in double-modulated THz-DTDS is not fundamental but can be reduced, in principle, by development of hardware that effectively increases the modulation frequency introduced by the spinning wheel. The spinning wheel measurement technique presented is of significance particularly for THz spectroscopy of liquids where the presence of noise is particularly problematic.

Acknowledgements

The authors thank Sigma Tools for technical assistance, Peter Cooke, Gretel Png, Shaghik Atakaramians, Doyeon Kim and Muammar Kabir for useful suggestions and discussions. We would like to acknowledge the support of the Australian Research Council (ARC) on the DP0556112 grant.

References

[1] G. Png, J. Choi, B.-H. Ng, S. Mickan, D. Abbott, X.-C. Zhang, Physics in Medicine and Biology 53 (13) (2008) 3501.
[2] P. Knobloch, C. Schildnecht, T. Kleine-Ostmann, M. Koch, S. Hoffmann, M. Hofmann, E. Rehberg, M. Sperling, K. Donhuijsen, G. Hein, K. Pierz, Physics in Medicine and Biology 47 (21) (2002) 3875.
[3] B. Fischer, H. Helm, P. Jepsen, Proceedings of the IEEE 95 (8) (2007) 1592.
[4] T. Globus, D. Woolard, T.W. Crowe, T. Khromova, B. Gelmont, J. Hesler, Journal of Physics D: Applied Physics 39 (15) (2006) 3405.
[5] L. Ho, R. Muller, M. Romer, K. Gordon, J. Heinamaki, P. Kleinebudde, M. Pepper, T. Rades, Y. Shen, C. Strachan, P. Taday, J. Zeitler, Journal of Controlled Release 119 (3) (2007) 253.
[6] Y.-S. Jin, S.-G. Jeon, G.-J. Kim, J.-I. Kim, C.-H. Shon, Review of Scientific Instruments 78 (2) (2007) 023101.
[7] G.-J. Kim, S.-G. Jeon, J.-I. Kim, Y.-S. Jin, Review of Scientific Instruments 79 (10) (2008) 106102.
[8] A.M. Sinyukov, Z. Liu, Y.L. Hor, K. Su, R.B. Barat, D.E. Gary, Z.-H. Michalopoulou, I. Zorych, J.F. Federici, D. Zimdars, Optics Letters 33 (14) (2008) 1593.
[9] K. Iwaszczuk, D.G. Cooke, M. Fujiwara, H. Hashimoto, P.U. Jepsen, Optics Express 17 (24) (2009) 21969.
[10] S.P. Mickan, R. Shvartsman, J. Munch, X.-C. Zhang, D. Abbott, Journal of Optics B: Quantum and Semiclassical Optics 6 (8) (2004) 786.
[11] Z. Jiang, M. Li, X.-C. Zhang, Applied Physics Letters 76 (22) (2000) 3221.
[12] S.P. Mickan, K.-S. Lee, T.-M. Lu, J. Munch, D. Abbott, X.-C. Zhang, Microelectronics Journal 33 (12) (2002) 1033.
[13] K.-S. Lee, T.-M. Lu, X.-C. Zhang, Microelectronics Journal 34 (1) (2003) 63.
[14] S.P. Mickan, A. Menikh, H. Liu, C.A. Mannella, R. MacColl, D. Abbott, J. Munch, X.-C. Zhang, Physics in Medicine and Biology 47 (21) (2002) 3789.
[15] J. Balakrishnan, B.M. Fischer, S. Mickan, D. Abbott, Novel T-ray liquid spectroscopy via double-modulated differential time-domain spectroscopy, in: Proceedings IRMMW-THz, Shanghai, China.
[16] W. Withayachumnankul, G.M. Png, X.X. Yin, S. Atakaramians, I. Jones, H.Y. Lin, B.S.Y. Ung, J. Balakrishnan, B.W.-H. Ng, B. Ferguson, S.P. Mickan, B. Fischer, D. Abbott, Proceedings of the IEEE 95 (8) (2007) 1528.
[17] J. Balakrishnan, B.M. Fischer, D. Abbott, Double-modulated DTDS-THz liquid spectroscopy using a novel spinning wheel technique, in: Proceedings IRMMW-THz, California, USA.
[18] J. Balakrishnan, B.M. Fischer, D. Abbott, IEEE Photonics Journal 1 (2) (2009) 88.
[19] L. Duvillaret, F. Garet, J.-L. Coutaz, IEEE Journal on Selected Topics in Quantum Electronics 2 (3) (1996) 739.
[20] J. Balakrishnan, B.M. Fischer, D. Abbott, Applied Optics 48 (13) (2009) 2262.
[21] B.M. Fischer, Broadband THz time-domain spectroscopy of biomolecules: a comprehensive study of the dielectric properties of biomolecules in the far-infrared (ch. 9, sec. 9.2), Ph.D. thesis, 2005.
[22] L. Duvillaret, F. Garet, J.-L. Coutaz, Proceedings of the SPIE–Terahertz Spectroscopy and Applications 3617 (1999) 38.
[23] W. Withayachumnankul, B.M. Fischer, D. Abbott, Optics Express 16 (10) (2008) 7382.
[24] R. Piesiewicz, C. Jansen, S. Wietzke, D. Mittleman, M. Koch, T. Kurner, International Journal of Infrared and Millimeter Waves 28 (5) (2007) 363.
[25] N. Nagai, R. Fukasawa, Chemical Physics Letters 388 (2004) 479.
[26] Y. Al-Ramadin, Optical Materials 14 (4) (2000) 287.
[27] T. Yasui, T. Araki, Japanese Journal of Applied Physics, Part 1: Regular Papers and Short Notes and Review Papers 44 (4 A) (2005) 1777.
[28] J. Son, J.V. Rudd, J.F. Whitaker, Optics Letters 17 (10) (1992) 733.
[29] A. Poppe, L. Xu, F. Krausz, C. Spielmann, IEEE Journal of Selected Topics in Quantum Electronics 4 (2) (1998) 179.